SUPPORTING INFORMATION

Experimental and theoretical investigation on the ORR activity of $AgVO_3$

Karuvatta Nubla[1$], Muhammed Fasil Puthiyaparambath[2$], Raghu Chatanathodi[2#], N. Sandhyarani[1]*

[1]Nanoscience Research Laboratory, School of Materials Science and Engineering,

[2]Department of Physics,

National Institute of Technology Calicut, Calicut, Kerala, India,

Tel.: 91 495 2286537, * E-mail: sandhya@nitc.ac.in

[#]raghuc@nitc.ac.in

[$]The authors contributed equally.

S1: Synthesis of Ag_2O and V_2O_5.

Synthesis of silver oxide

To a 0.5M NaOH solution, 0.1M $AgNO_3$ in 40 ml DI water was added and stirred the reaction mixture for 2 hrs at room temperature. A black-colored precipitate was formed, which was centrifuged, washed with DI water followed by ethanol, and dried overnight.

Synthesis of vanadium oxide

Vanadium oxide has been synthesized by making slight changes in a reported procedure[1]. Briefly, 0.1M NH_4VO_3 was prepared in 40 ml DI water. To this, CTAB was added and kept for stirring. 0.1M HNO_3 was added to the reaction mixture. Then, a hydrothermal reaction was carried out at

180˚C for 24 hours. Centrifuged, washed, and dried the reddish-colored precipitate. Then, calcined at 500˚C for 2 hours.

The crystal structures of the synthesized Ag_2O and V_2O_5 were examined by X-ray diffraction technique and shown in Figures S1 (A) and (B), respectively. XRD pattern of Ag_2O exhibited distinct diffraction peaks at the two theta values 26.6˚, 32.7˚, 37.9˚, 54.8˚,65.4˚, and 68.7˚ can be indexed to the (110), (111), (200), (220), (311) and (222) crystallographic planes of cubic Ag_2O (JCPDS # 00-012-0793)[2]. XRD pattern of vanadium oxide displayed diffraction peaks at the two theta values 15.3˚, 20.1˚, 21.7˚, 26.1˚, 30.9˚, 32.4˚, 33.2˚, 34.2˚, 36.01˚, 37.3˚, 41.2˚, 42˚, 45.4˚, 47.2˚, 47.7˚, 48.8˚, 49.5˚, 51.1˚, 52˚, 55.6˚, 61.1˚, 62.1˚, which could be ascribed to the (200), (001), (101), (110), (400), (011), (111), (310), (211), (401), (002), (102), (411), (600), (302), (012), (112), (020), (601), (021), (321) and (710) crystallographic planes are in accordance with the standard data of orthorhombic V_2O_5 (JCPDS #00-009-0387)[3,4].

Cyclic voltammetry of the synthesized Ag_2O and V_2O_5 was carried out to understand the electrochemical activity of the catalysts towards ORR in O_2 and N_2 saturated 0.1M KOH solution, which is shown in Figure S1 (C). In O_2 saturated solution, both catalysts exhibited an oxygen reduction peak. LSV experiments were also conducted in 0.1M O_2 saturated KOH media to study the ORR activities of these catalysts and is given in Figure 1 (D) and (E). From the results, it was observed that the ORR performance of the mixed transition metal oxide ($AgVO_3$) is higher than that of the individual oxides (Ag_2O and V_2O_5) in terms of onset potential and in current density.

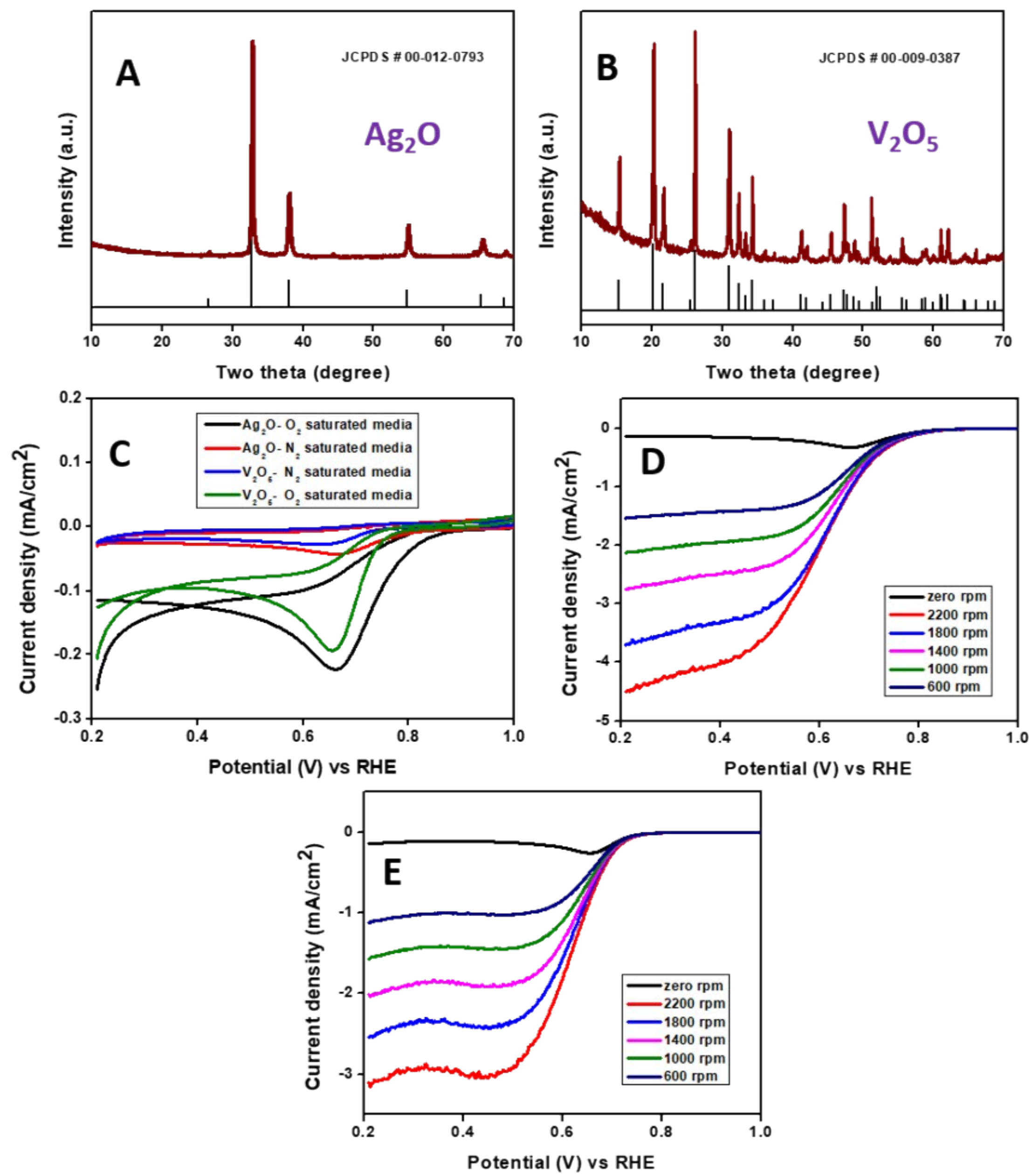

Figure S1: XRD spectrum of (A) silver oxide (B) vanadium oxide (C) Cyclic Voltammogram of Ag_2O and V_2O_5 in O_2 saturated, and N_2 saturated 0.1M KOH solution (D) and (E) Linear Sweep Voltammogram of Ag_2O and V_2O_5 at different rpm in O_2 saturated 0.1M KOH solution respectively.

S2: The detailed reaction scheme of ORR in alkaline media

The 4e$^-$ process proceeds through the following steps, if the process is associative:

$$O_2(g) + H_2O\ (l) + e^- + * \rightarrow OOH^* + OH^- \quad (1)$$

$$OOH^* + e^- \rightarrow O^* + OH^- \quad (2)$$

$$O^* + H_2O\ (l) + e^- \rightarrow OH^* + OH^- \quad (3)$$

$$OH^* + e^- \rightarrow OH^- \quad (4)$$

Where * refers to the active site of $AgVO_3$, (g) and (l) refers to gas and liquid phases, respectively.

If dissociative:

$$O_2(g) + * \rightarrow 2O^* \quad (5)$$

$$O^* + H_2O\ (l) + e^- \rightarrow OH^* + OH^- \quad (6)$$

$$OH^* + e^- \rightarrow OH^- \quad (7)$$

The adsorption energies of OOH, O, and OH are calculated relative to H_2O and H_2. They are given by

$$\Delta E_{OOH*} = (E_{OOH*} - E_*) - (2\,E_{H_2O} - {}^3/_2 E_{H_2}) \quad (8)$$

$$\Delta E_{O*} = (E_{O*} - E_*) - (E_{H_2O} - E_{H_2}) \quad (9)$$

$$\Delta E_{OH*} = (E_{OH*} - E_*) - (E_{H_2O} - {}^1/_2 E_{H_2}) \quad (10)$$

Table S1: Adsorption energy of (E_{ads}) of O_2 adsorbed on alpha $AgVO_3$.

$AgVO_3$-Site	E_{ads} (eV)	$d_{M\text{-}O}$ (Å)	$d_{O\text{-}O}$ (Å)
Ag	-0.12	2.37	1.26
V	-0.97	1.98	1.33

Table S2: Adsorption energy and Bader charge of various ORR intermediates. $d_{M\text{-}O}$ indicates the distance between metal and oxygen atom. Bader analysis has been performed on the ground state charge density obtained from a DFT calculation upon adsorption of the species on the adsorption site.

Intermediates	E_{ads} (eV)	$d_{M\text{-}O}$ (Å)	Charge (e^-)
O_2	-0.97	1.98	-0.43
OOH	-2.28	1.85	-0.48
O	-4.10	1.65	-0.72
OH	-3.42	1.81	-0.40

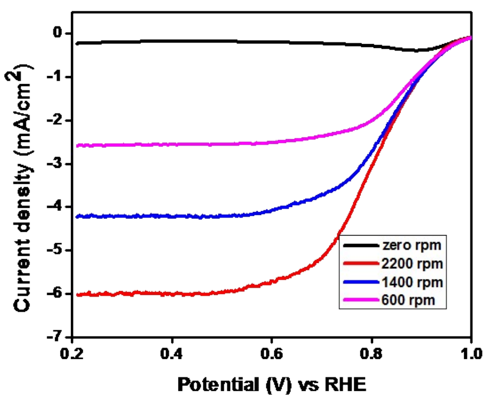

Figure S2: LSV of commercial Pt/C in O_2 saturated 0.1M KOH

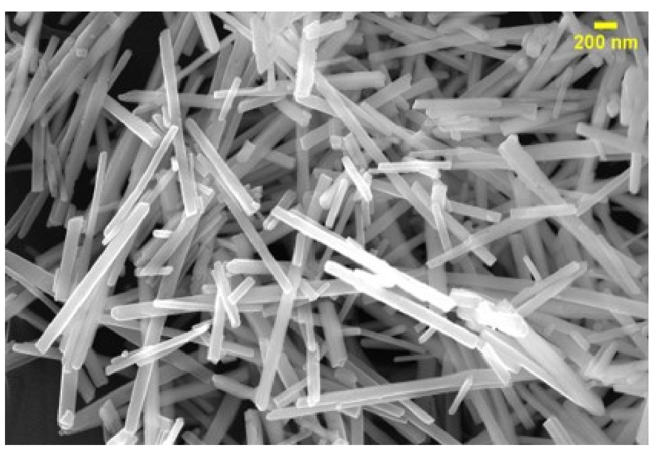

Figure S3: FE-SEM image of $AgVO_3$ after the accelerated durability test

S3: MEA fabrication

The pretreated Nafion 117 was used as the membrane. The pretreatment approach includes the subsequent heating of the Nafion in H_2O_2 followed by H_2SO_4 and then DI water. Two sets of MEA were prepared, one with Pt-Ru (1:1)/C as anode and Pt/C as cathode, second with Pt-Ru (1:1)/C as anode and $AgVO_3$ as the cathode. Carbon cloths were cut into 5cm x 5 cm dimensions. Carbon black was suspended in DI water + IPA mixture containing nafion binder to prepare the microporous layer and then kept for sonication for 1 hour. The slurry was coated on the PTFE (polytetrafluoroethylene) treated carbon cloth using a paintbrush. Catalyst ink was prepared by dispersing appropriate catalyst in DI water + IPA with Nafion binder and then coated on respective carbon cloth and dried. The loading of the anode and cathode catalysts on the carbon cloth was 3.5 mg/cm^2 and 2 mg/cm^2, respectively. The MEA was made by sandwiching the Nafion 117 membrane between anode and cathode catalyst coated carbon cloth and hot pressing it at 100˚C and 76 kg/cm^2. The MEA was then applied to a passive air-breathing direct methanol fuel cell (DMFC), and a 1M methanol solution was injected into the anodic compartment. For the OCV measurements, DMFC was connected to a multimeter and noted the OCV at different time intervals. The OCV vs. time plot is given in Figure S4. $AgVO_3$ cathode reached an OCV of 0.427V, which comes in the region of Pt/C cathode (0.481V), indicating the effectiveness of the reported catalyst.

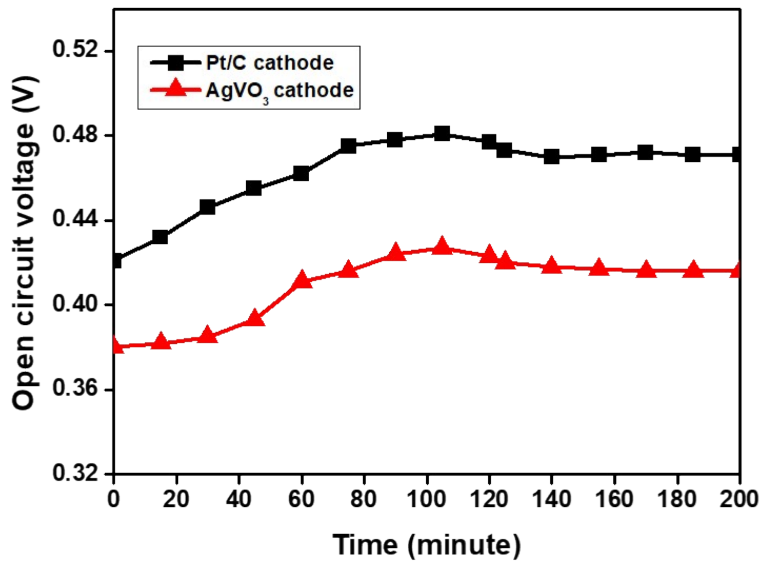

Figure S4: Comparison of the OCV of DMFC with Pt/C and $AgVO_3$ cathode

Table S3: Comparison of ORR activity of $AgVO_3$ with different MTMOs reported in the literature

Sl. No.	Catalyst material	Electrolyte	Onset Potential (V)	Current density @ 1600 rpm, mA/cm^2	Reference
1	$Co_3Mo_2O_xN_{6-x}/C$	0.1M KOH	0.9 V (RHE)	-5.5	[5]
2	$ZnCo_2O_4$	0.1M KOH	0.83 V (SHE)	-2.97	[6]
3	$ZnMnCoO_4$	0.1M KOH	0.94 V (SHE)	-5.22	[6]
4	$CuCo_2O_4$/N-rGO	1M KOH	-0.14 V (SCE)	-3.4	[7]
5	$MnCo_2O_4$/N-rmGO	1M KOH	0.95 (RHE)	-3.7	[8]
6	Silver-molybdate	1M KOH	-	-2.0	[9]
7	$Ag/Mn_3O_4/C$	0.1M NaOH	-	-5.43	[10]
8	$LaMn_{0.7}Co_{0.3}O_3$	0.1M KOH	0.88 V (RHE)	-3.4	[11]
9	$LaCoO_3$	1M KOH	-0.2 V (Ag/AgCl)	-3.5	[12]

10	$LaMnO_3$	1M KOH	-0.12 V (Ag/AgCl)	-4.0	[12]
11	$NdCuO_x$@CN	0.1M KOH	0.015 V (Ag/AgCl)	-3.41	[13]
12	$CoFe_2O_4$	0.1M KOH	0.85 V (RHE)	-5.0	[14]
13	$MnFe_2O_4$	0.1M KOH	0.88 V (RHE)	-4.70	[14]
14	$NiFe_2O_4$	0.1M KOH	0.81 V (RHE)	-4.95	[14]
15	$NiCoMnO_4$	0.1M KOH	0.87 V (RHE)	-4.0	[15]
16	$ZnCo_2O_4$	1M KOH	0.81 V (RHE)	-	[16]
17	Al-substituted $MnFe_2O_4$/rGO	0.1M KOH	0.92 V (RHE)	-3.0	[17]
18	Mn_3O_4/NCNTs/Co	0.1M KOH	0.94 V(RHE)	-5.7	[18]
19	$ZnCo_2O_4$	0.1M KOH	0.77 V (RHE)	-3.0	[19]
20	Ag-$MnFe_2O_4$/NG	0.1M KOH	0.886 V (RHE)	-4.0	[20]
21	Ag-$MnFe_2O_4$/NSG	0.1M KOH	0.908 V (RHE)	-6.0	[20]
22	N-$CuCo_2O_4$@CNF	0.1M KOH	0.89 V (RHE)	-6.9	[21]
23	NiO/$NiCo_2O_4$	KOH	0.89V (RHE)	-4.77	[22]
24	$NiCo_2O_4$	0.1M KOH	0.91 V (RHE)	-3.42	[23]
25	$CoMn_2O_4$/NC	0.1M KOH	0.93 V (RHE)	-5.2	[24]
26	$La_{0.8}Sr_{0.2}MnO_{3-\delta}$ / CFC	0.1M KOH	0.866V (RHE)	-4.86	[25]
27	**$AgVO_3$**	**0.1M KOH**	**0.82 (RHE)**	**-5.0**	This work

References

(1) Vishnuprakash, P.; Nithya, C.; Premalatha, M. Exploration of V_2O_5 Nanorod@rGO Heterostructure as Potential Cathode Material for Potassium-Ion Batteries. *Electrochimica Acta* **2019**, *309*, 234–241.

(2) Kim, M.-J.; Cho, Y.-S.; Park, S.-H.; Huh, Y.-D. Facile Synthesis and Fine Morphological Tuning of Ag_2O. *Cryst. Growth Des.* **2012**, *12* (8), 4180–4185.

(3) Babar, B. M.; Mohite, A. A.; Patil, V. L.; Pawar, U. T.; Kadam, L. D.; Kadam, P. M.; Patil, P. S. Sol-Gel Prepared Vanadium Oxide for Photocatalytic Degradation of Methylene Blue Dye. *Mater. Today Proc.* **2021**, *43*, 2673–2677.

(4) Wang, Y. Zhihu Pan, Xiaohong Ji, Ti_3C_2Tx (MXene)-Wrapped V_2O_5/Fe_2O_3 Composites for Enhanced-Performance Supercapacitors. New J. Chem., **2022**, 46, 7704

(5) An, L.; Xia, Z.; Chen, P.; Xia, D. Layered Transition Metal Oxynitride $Co_3Mo_2O_xN_{6-x}$ /C Catalyst for Oxygen Reduction Reaction. *ACS Appl. Mater. Interfaces* **2016**, *8* (43), 29536–29542.

(6) Baby, A.; Senthilkumar, B.; Barpanda, P. Low-Cost Rapid Template-Free Synthesis of Nanoscale Zinc Spinels for Energy Storage and Electrocatalytic Applications. *ACS Appl. Energy Mater.* **2019**, *2* (5), 3211–3219.

(7) Ning, R.; Tian, J.; Asiri, A. M.; Qusti, A. H.; Al-Youbi, A. O.; Sun, X. Spinel $CuCo_2O_4$ Nanoparticles Supported on N-Doped Reduced Graphene Oxide: A Highly Active and Stable Hybrid Electrocatalyst for the Oxygen Reduction Reaction. *Langmuir* **2013**, *29* (43), 13146–13151.

(8) Liang, Y.; Wang, H.; Zhou, J.; Li, Y.; Wang, J.; Regier, T.; Dai, H. Covalent Hybrid of Spinel Manganese–Cobalt Oxide and Graphene as Advanced Oxygen Reduction Electrocatalysts. *J. Am. Chem. Soc.* **2012**, *134* (7), 3517–3523.

(9) Wang, Y.; Liu, Y.; Lu, X.; Li, Z.; Zhang, H.; Cui, X.; Zhang, Y.; Shi, F.; Deng, Y. Silver-Molybdate Electrocatalysts for Oxygen Reduction Reaction in Alkaline Media. *Electrochem. Commun.* **2012**, *20*, 171–174.

(10) Tang, Q.; Jiang, L.; Qi, J.; Jiang, Q.; Wang, S.; Sun, G. One Step Synthesis of Carbon-Supported Ag/Mn_yO_x Composites for Oxygen Reduction Reaction in Alkaline Media. *Appl. Catal. B Environ.* **2011**, *104* (3–4), 337–345.

(11) Liu, X.; Gong, H.; Wang, T.; Guo, H.; Song, L.; Xia, W.; Gao, B.; Jiang, Z.; Feng, L.; He, J. Cobalt-Doped Perovskite-Type Oxide $LaMnO_3$ as Bifunctional Oxygen Catalysts for Hybrid Lithium-Oxygen Batteries. *Chem. - Asian J.* **2018**, *13* (5), 528–535.

(12) Ashok, A.; Kumar, A.; Bhosale, R. R.; Almomani, F.; Malik, S. S.; Suslov, S.; Tarlochan, F. Combustion Synthesis of Bifunctional $LaMO_3$ (M = Cr, Mn, Fe, Co, Ni) Perovskites for Oxygen Reduction and Oxygen Evolution Reaction in Alkaline Media. *J. Electroanal. Chem.* **2018**, *809*, 22–30.

(13) Song, J.; Wang, W.; Wang, F.; Kang, Y.; Liu, S.; Lei, Z. Encapsulated NdCuOx Bimetallic Nanoparticles with Nitrogen Doped Carbon as an Efficient Electrocatalyst for Oxygen Reduction Reaction. *Electrochimica Acta* **2017**, *258*, 1404–1412.

(14) Si, C.; Zhang, Y.; Zhang, C.; Gao, H.; Ma, W.; Lv, L.; Zhang, Z. Mesoporous Nanostructured Spinel-Type MFe_2O_4 (M = Co, Mn, Ni) Oxides as Efficient Bi-Functional Electrocatalysts towards Oxygen Reduction and Oxygen Evolution. *Electrochimica Acta* **2017**, *245*, 829–838.

(15) Pendashteh, A.; Palma, J.; Anderson, M.; Marcilla, R. $NiCoMnO_4$ Nanoparticles on N-Doped Graphene: Highly Efficient Bifunctional Electrocatalyst for Oxygen Reduction/Evolution Reactions. *Appl. Catal. B Environ.* **2017**, *201*, 241–252.

(16) Sankalpita Chakrabarty, AyanMukherjee, Wei-NienSu, Suddhasatwa Basu, Improved bi-functional ORR and OER catalytic activity of reduced graphene oxide supported $ZnCo_2O_4$ microsphere, *Int. J. Hydrog. Energy,* 44, **2019**, 1565-1578

(17) Tyagi, A.; Penke, Y. K.; Sinha, P.; Malik, I.; Kar, K. K.; Ramkumar, J.; Yokoi, H. ORR Performance Evaluation of Al-Substituted $MnFe_2O_4$/ Reduced Graphene Oxide Nanocomposite. *Int. J. Hydrog. Energy* **2021**, *46* (43), 22434–22445.

(18) Lu, L.-N.; Chen, C.; Xiao, K.; Ouyang, T.; Zhang, J.; Liu, Z.-Q. Boosting Oxygen Electrocatalytic Reactions with Mn_3O_4 /Self-Growth N-Doped Carbon Nanotubes Induced by Transition Metal Cobalt. *Catal. Sci. Technol.* **2020**, *10* (21), 7256–7261.

(19) Sreekanth, T. V. M.; Nagajyothi, P. C.; Devarayapalli, K. C.; Shim, J.; Yoo, K. Lilac Flower-Shaped ZnCo $_2$ O $_4$ Electrocatalyst for Efficient Methanol Oxidation and Oxygen Reduction Reactions in an Alkaline Medium. *CrystEngComm* **2020**, *22* (16), 2849–2858.

(20) Chen, Y.; Shi, Z.; Li, S.; Feng, J.; Pang, B.; Yu, L.; Zhang, W.; Dong, L. N, S-Codoped Graphene Supports for Ag-$MnFe_2O_4$ Nanoparticles with Improved Performance for Oxygen Reduction and Oxygen Evolution Reactions. *J. Electroanal. Chem.* **2020**, *860*, 113930.

(21) Zhang, Y.; Chen, Z.; Tian, J.; Sun, M.; Yuan, D.; Zhang, L. Nitrogen Doped $CuCo_2O_4$ Nanoparticles Anchored on Beaded-like Carbon Nanofibers as an Efficient Bifunctional Oxygen Catalyst toward Zinc-Air Battery. *J. Colloid Interface Sci.* **2022**, *608*, 1105–1115.

(22) Zhang, Z.; Liang, X.; Li, J.; Qian, J.; Liu, Y.; Yang, S.; Wang, Y.; Gao, D.; Xue, D. Interfacial Engineering of NiO/$NiCo_2O_4$ Porous Nanofibers as Efficient Bifunctional Catalysts for Rechargeable Zinc–Air Batteries. *ACS Appl. Mater. Interfaces* **2020**, *12* (19), 21661–21669.

(23) Béjar, J.; Álvarez-Contreras, L.; Ledesma-García, J.; Arjona, N.; Arriaga, L. G. Electrocatalytic Evaluation of Co_3O_4 and $NiCo_2O_4$ Rosettes-like Hierarchical Spinel as Bifunctional Materials for Oxygen Evolution (OER) and Reduction (ORR) Reactions in Alkaline Media. *J. Electroanal. Chem.* **2019**, *847*, 113190.

(24) Ho, J.; Li, Y.; Dai, Y.; Kim, T.; Wang, J.; Ren, J.; Yun, H.; Liu, X. Ionothermal Synthesis of N-Doped Carbon Supported $CoMn_2O_4$ Nanoparticles as ORR Catalyst in Direct Glucose Alkaline Fuel Cell. *Int. J. Hydrog. Energy* **2021**, *46* (39), 20503–20515.

(25) Changjing Fu , Qiang Ma1, Qibing Wu , Zaifang Yuan , Jun He, Effects of Silver Modification of $La_{0.8}Sr_{0.2}MnO_{3-\delta}$ Cathode on the Catalytic Activity for the Oxygen Reduction Reaction in a Flexible Al-Air Battery. *Int. J. Electrochem. Sci.* **2020**, 9473–9486.